On the Nature of the 1994 East Asian Summer Drought

CHUNG-KYU PARK

Forecast Bureau, Korea Meteorological Administration, Seoul, Korea

SIEGFRIED D. SCHUBERT

Data Assimilation Office, Laboratory for Atmospheres, NASA/Goddard Space Flight Center, Greenbelt, Maryland

(Manuscript received 29 December 1995, in final form 14 August 1996)

ABSTRACT

East Asian countries experienced record-breaking heat waves and drought conditions during the summer monsoon season of 1994. This study documents the large-scale circulation associated with the drought and suggests a forcing mechanism responsible for the anomalous evolution of the East Asian monsoon. The results, based on Goddard Earth Observing System (GEOS) global assimilated data for 1985–94, indicate that the absence of monsoon rainfall during July 1994 over central China and the southern parts of Korea and Japan is due to the unusually early development of the climatological upper-level anticyclonic flow east of the Tibetan Plateau. The anomalous July anticyclonic circulation over the East Asian–northwestern Pacific region and the cyclonic circulation over the subtropical western Pacific, which are more typical of August, acted to reduce the moisture supply from the western Pacific and the Indian Ocean leading to suppressed rainfall over East Asia. The similarity of the July 1994 East Asian circulation anomalies to the climatological July to August change in these quantities suggests that the anomalies may be viewed as an acceleration of the seasonal cycle in which the circulation transitions to August conditions earlier than normal.

Neither tropical nor middle latitude SST anomalies provide a viable forcing mechanism for the 1994 East Asian circulation anomalies: the tropical anomalies are weak and the middle latitude anomalies, while stronger, appear to be primarily a response to atmospheric forcing, though they may feed back to reinforce the atmospheric anomalies. It is suggested, instead, that the anomalous circulation is primarily the result of an orographic forcing associated with zonal wind changes over Tibet. The zonal wind change, characterized by an anomalous northward shift of the East Asian jet is, in turn, tied to unusually persistent stationary waves extending from northern Europe, which developed prior to the onset of the East Asian anticyclone. Several other occurrences of atmospheric anomalies similar in structure (though weaker in amplitude) to the July 1994 anomalies are found in the previous nine summers, suggesting the operative mechanism is not unique to 1994. Such a mechanism appears to operate both for the climatological development of the ridge and for the occurrences of similar anomalies in previous summers: in the former the northward shift of the jet over Tibet is a reflection of climatological seasonal change in the zonal wind, while in the latter, the shift is the result of anomalies similar in structure to the 1994 European–Asian wave pattern.

The indirect role of the Eurasian waves in the development of the East Asian circulation anomalies suggests that useful monthly and longer predictions of the monsoon rests, not only on our ability to predict the occurrence of these waves, but also on our ability to properly model their interaction with orography.

1. Introduction

The monsoon is basically a response of the atmosphere to the differential heating between the land mass of the Asian continent and the adjacent oceans. The atmospheric response, however, may be quite complicated due to the interactions between the atmospheric heat sources, land–sea contrast, and topography. The East Asian monsoon exhibits a particularly complex seasonal behavior resulting from a combination of strong tropical and middle latitude influences. For example, in June the East Asian monsoon trough starts to show both midlatitude frontal and tropical ITCZ-like (intertropical convergence zone) properties followed by a northward jump of the elongated rain belt to the Yantze River valley. As the quasi-stationary rain belt jumps into the Huaihe River basin in July, the East Asian countries are normally under the influence of a stationary rain belt, which is referred to as Baiu in Japan and Changma in Korea.

The Asian summer monsoon has a profound social and economic impact in East Asia and its surrounding countries. While the above monsoon evolution is largely phase-locked with the seasonal cycle, a failure of this climatological monsoon evolution is not unusual. Of

Corresponding author address: Dr. Chung-Kyu Park, Korea Meteorological Administration, 1 Songwol-dong, Chongno-gu, Seoul 110-101, Korea.

particular concern to society are hydrologic disasters such as floods and severe droughts, which are often connected with stagnated large-scale circulation systems. The recent devastating drought over the East Asian countries (the southern half of Korea, Japan, and central China) in the summer of 1994 (World Meteorological Organization 1995), in particular, highlights the range of variability in the progress of the monsoon. The forcing mechanisms responsible for such an extreme failure of the monsoon are yet to be understood.

A number of studies have examined the large-scale coupling between the monsoon and the ocean surface anomalies associated with El Niño/La Niña. For example, Nigam (1994) studied the dynamical basis for the Asian summer monsoon rainfall–El Niño linkage through diagnostic calculations with a linear steady-state multilayer primitive equation model. His diagnostic analysis suggests that the orographically forced circulation anomaly due to the changes in the zonally averaged basic state are important in modulating the low-level moisture flux convergence and hence monsoon rainfall over Indochina. The El Niño phenomenon has been shown empirically to be linked to deficient summer monsoon rainfall over India and to interannual rainfall fluctuations in the global Tropics and extratropics (Ropelewski and Halpert 1987). Anomalous Asian summer monsoon rainfall, on the other hand, appears to impact El Niño/La Niña development via modulation of the near-surface flow over the tropical Pacific (Meehl 1994; Webster and Yang 1992; Yasunari 1991). Yasunari (1991) showed evidence that anomalies in rainfall and circulation associated with the monsoon/El Niño–Southern Oscillation (ENSO) system tend to be phase-locked to the annual cycle with the anomalies changing sign during the late spring to early summer period.

The significance of the Tibetan Plateau as an elevated heat source for the evolution of the Asian summer monsoon circulation has been discussed by many authors (e.g., Ye 1981; Murakami 1987; Yanai et al. 1992; Yanai and Li 1994). The sensible heat flux from the surface provides the major source of heating on the plateau. However, additional contributions from condensation heating occur over the eastern plateau during summer. A number of GCM studies also suggest the importance of topography in the sudden northward shift of the wind belt (Hahn and Manabe 1975; Broccoli and Manabe 1992). Recently, Ting (1994) used a linear baroclinic model to separate the effect of various stationary wave forcings obtained from the GFDL GCM simulation and to study the relative roles of diabatic heating and the orographic forcing in maintaining the summer stationary waves. That study found that most of the subtropical stationary wave features in the GCM can be explained by the response to diabatic heating, particularly in the Asian monsoon regions. The stationary nonlinearity due to the interaction between thermally driven monsoon flow and the orography was found to be largely responsible for the extratropical, equivalent barotropic stationary wave features over the Tibetan Plateau and the North American continent.

In addition to documenting the circulation anomalies associated with the 1994 East Asian summer drought, this study will determine whether the observations are consistent with the hypothesis that the anomalous July anticyclonic circulation over East Asia is orographically forced. The study employs various assimilated datasets produced by version 1 of the Goddard Earth Observing System (GEOS-1) data assimilation system. These include a multiyear reanalysis (for the period 1985–93, Schubert et al. 1993) and a special assimilation experiment run for the summer of 1994. The GEOS-1 data assimilation system is described briefly in the appendix. A description of the circulation features and accompanying sea surface temperatures are presented in section 2. Section 3 examines possible forcing mechanisms. Section 4 puts the 1994 anomalies in perspective by examining the anomalies during the entire 9-yr record available from the GEOS-1 assimilation, and the conclusions are given in section 5.

2. Circulation features

In this section we present the circulation patterns for the northern summer. We also present the accompanying SST fields and selected components of the hydrologic cycle. Since our argument for the causes of the 1994 East Asian drought centers on this event being an anomalous manifestation of the seasonal cycle, we focus first on the summertime seasonal changes, and then on the 1994 circulation anomalies.

a. Climatology

Figure 1 shows the July and August climatology patterns of the eddy height and jet maxima at the 200-mb level. The climatologies are obtained from the 9-yr (1985–93) average of the GEOS analyses. The July stationary wave pattern in the Northern Hemisphere is dominated by the Tibetan anticyclone and the two mid-ocean upper-level troughs with maximum amplitude near 30°N. There are two upper-tropospheric anticyclonic centers in the Asian area, one located over the Tibetan Plateau, the other over the Iran–Afganistan region. In July, the dominant anticyclone is found over the region from the western part of the Tibetan Plateau to Iran. This anticyclonic center weakens in August as the sensible heat flux from the surface and additional contributions from condensation heating provide the major source of heating on the plateau. The subtropical jet axis is found around the northern edge of the Tibetan anticyclone with enhanced wind speeds associated with the local high and low pressure centers. The East Asian subtropical jet is extended eastward with a local maximum off the east coast of Japan associated with a trough located south of the Kamchatka peninsula. The stationary wave pattern in August is generally similar to that

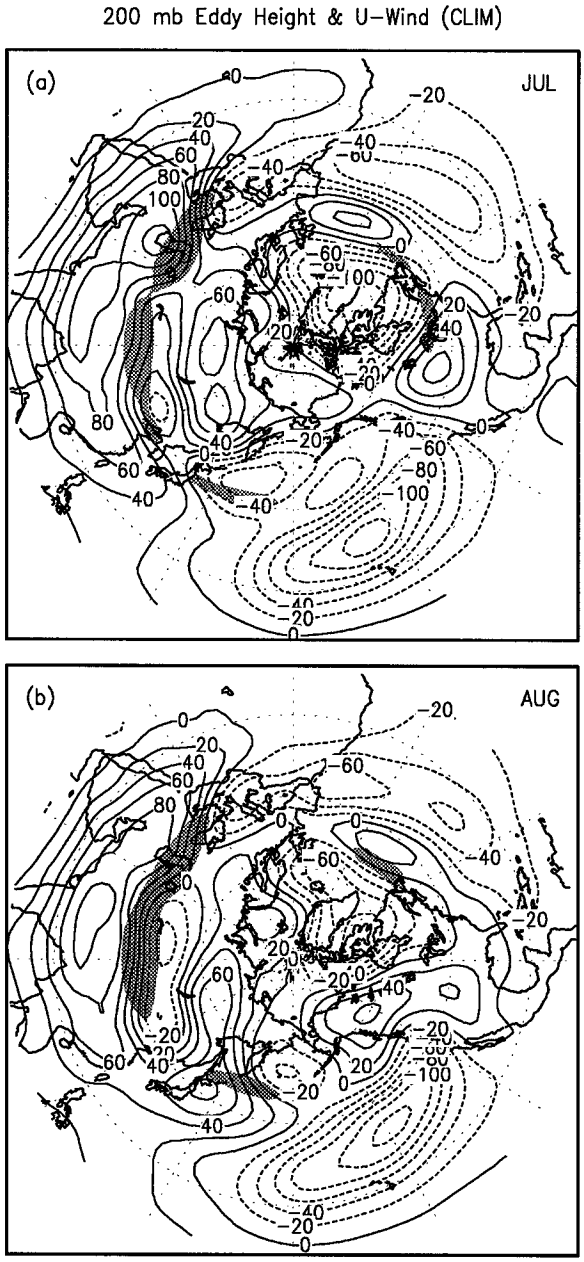

FIG. 1. (a) July and (b) August climatology (1985–93) of the eddy height and u-wind at the 200-mb level. Contour interval is 20 m. Dotted lines represent the negative values. Shading represents the u-wind greater than 25 m s^{-1}.

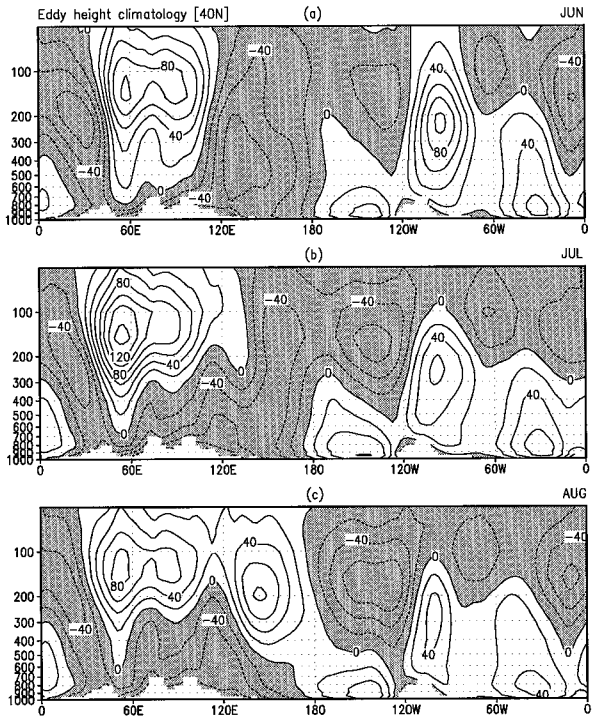

FIG. 2. Longitude-pressure sections of the eddy height climatology at 40°N for (a) June, (b) July, and (c) August. Contour interval is 20 m. Negative regions are shaded.

of July. There is a northeastward shift of the midocean troughs in the subtropics and northwestward displacement of the ridge over North America. The major difference, however, is the pronounced change over the northwestern Pacific region where the upper-level trough is replaced by ridge in August. The East Asian jet is shifted farther north as the anticyclonic circulation dominates the northwestern Pacific region off the east coast of Japan.

The longitude-pressure sections of the eddy height climatology at 40°N in Fig. 2 better illustrate the seasonal evolution of the middle latitude stationary waves. While the seasonal evolution of the upper-level anticyclonic flow around the Tibetan Plateau (the Tibetan high) is a dominant feature in the Eastern Hemisphere during the summer, the cross sections at 40°N in Fig. 2 emphasize the evolution of stationary waves over the East Asian sector; this is at the northern periphery of the Tibetan anticyclone. The most pronounced seasonal evolution in August is the rapid development of the anticyclone near 150°E, which is somewhat separated from the Tibetan anticyclone. The development of the upper-level anticyclone east of Tibet substantially changes the middle latitude circulation in the Eastern Hemisphere including the vertical structure, which shows a strong dipole over the western Pacific around 150°E in August. While Fig. 2 gives the impression that the East Asian anticyclone is simply an eastward extension of the Tibetan anticyclone, the nature of their relationship is unclear. In the Western Hemisphere, the seasonal evolution is characterized by the gradual development of an upper-level trough over the eastern Pacific (130°W) and weakening of the ridge over North America (110°W).

The main source of the low-level moisture that sustains the East Asian monsoon is still a subject of debate. Figure 3a shows the July climatology of the sea level pressure, the vertically integrated moisture flux, and

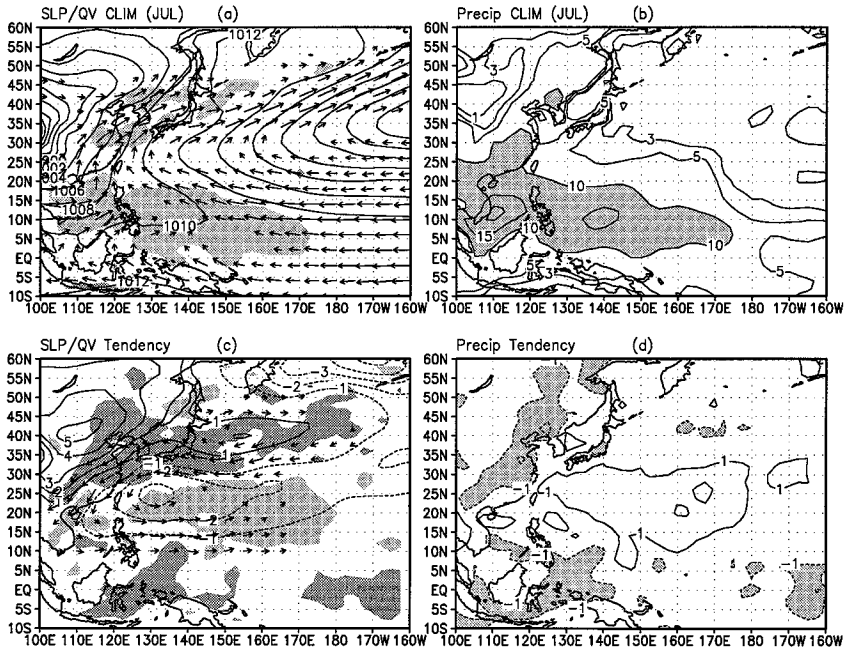

FIG. 3. (a) Sea level pressure (contoured), vertically integrated moisture flux (vectors), moisture convergence (shading), and (b) precipitation for the July climatology. Same quantities for the difference between July and August climatology (August–July) are shown in (c) and (d). Contour intervals are 2 mb in (a) and 1 mb in (c). In (a), shading represents the moisture convergence greater than 4 mm day^{-1}. In (c), darker shading represents the values less than -1 mm day^{-1} and lighter shading represents the values greater than 1 mm day^{-1}. The vectors are in the unit of g kg^{-1} m s^{-1} with arbitrary size. Contours for precipitation are -3, -1, 1, 3, 5, 10, 15, and 20 mm day^{-1}.

moisture convergence. This figure suggests that the primary moisture source for the summer rainfall over East Asia originates in two airflows: the Indian summer monsoonal airflow and the southeast monsoon coming from the southern flank of the subtropical high over the western Pacific. There is a weak contribution from the cross-equatorial air flowing over Southeast Asia and the South China Sea, which originates in the Australian region. It is often observed that one branch of the above three monsoon airflows or combinations thereof may affect the area (Ding 1994). Figure 3a shows that the sea level pressure patterns over east China and the North Pacific are good indicators of the northward moisture transport over East Asia. As shown in Figs. 3a and 3b, the moisture supplied by the zonal component of the winds in the Tropics is important for the heavy rainfall over the western Pacific at around 10°N.

Figures 3a and 3b also indicate that in the Tropics the assimilation is providing a physically consistent picture with heavy rainfall in the regions of strong moisture convergence. On the other hand, the region of strong moisture convergence along the northern periphery of the subtropical high stretching from east China to the central North Pacific is not balanced by the difference between evaporation and precipitation (not shown). The imbalance in this case is largely explained by the additional moisture tendency (analysis increment) associated with the assimilation process (see Molod et al. 1996). The absence of the monsoon rainband appears to be a problem associated with model parameterizations. Since the winds and moisture are directly analyzed in the data assimilation process, the vertically integrated moisture flux (on the model's sigma levels) is considered more reliable than other parameterized hydrologic quantities.

The tendency pattern in Fig. 3c suggests that the most significant reduction of the moisture convergence (darker shading) over the Korea and Japan region in August is associated with positive pressure changes over northern China and east of Japan and the negative pressure changes over the subtropical western Pacific off the east coast of south China. The seasonal pressure changes over the Asian–Pacific region results in substantial reductions in the moisture convergence and rainfall over East Asia, while enhancing the rainfall over the western and central Pacific at around 25°N in August (Fig. 3d), which is consistent with the enhanced moisture convergence (lighter shading) in Fig. 3c.

Figure 4 shows the 200-mb height and SST monthly tendencies during the northern summer. The height tendencies from June to July (Fig. 4a) and from August to September (Fig. 4c) are dominated by positive and negative tendencies in the zonal mean component, representing hemispheric warming and cooling, respectively.

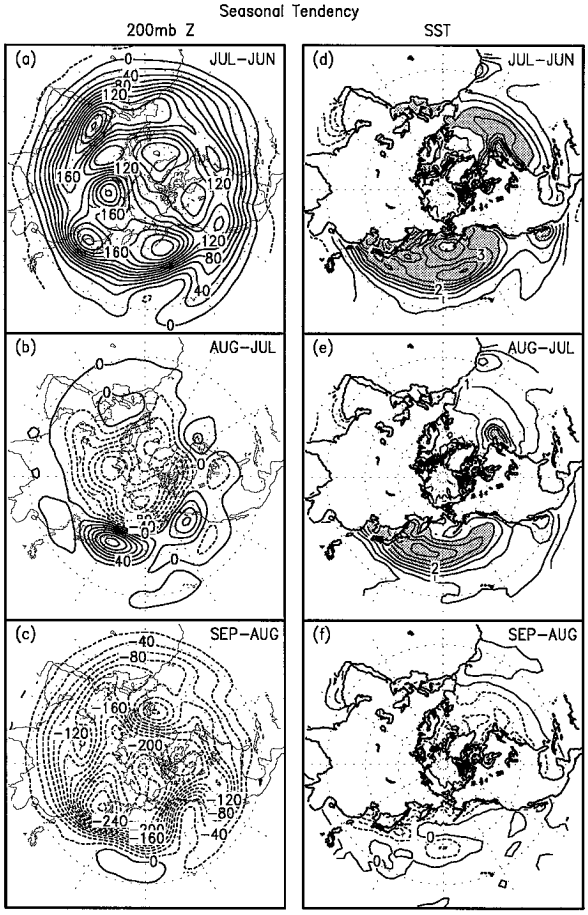

FIG. 4. The 200-mb height climatology difference for (a) July–June, (b) August–July, and (c) September–August, and the SST climatology difference for (d) July–June, (e) August–July, and (f) September–August. Contour interval is 20 m for the height and 0.5 °C for SST. Dotted lines represent the negative values. The values greater than 2.5°C are shaded for SST.

There are, however, substantial local maxima imbedded in the zonal mean changes. These maxima tend to occur near 40°N throughout the Northern Hemisphere. Especially relevant for this study are the enhanced positive tendencies from June to July (Fig. 4a) extending from the Iran–Afghanistan region across much of the Asian continent, and the local maximum over the east coast of Asia. Between July and August (Fig. 4b) the local tendency is the dominant change in the middle latitude circulation and results in the replacement of the trough located south of the Kamchatka peninsula with a ridge in August, as noted earlier. The northwest displacement of the ridge over central North America in August (Fig. 1b) is responsible for the strong positive tendency over the Gulf of Alaska and the negative tendency near the Great Lakes in Fig. 4b. During this time, the higher latitudes are marked by a strong zonally symmetric negative tendency marking the onset of the seasonal cooling in the Northern Hemisphere. The negative height tendencies extend southward east of the Caspian Sea in association with the weakening of the center of the Tibetan high over Iran.

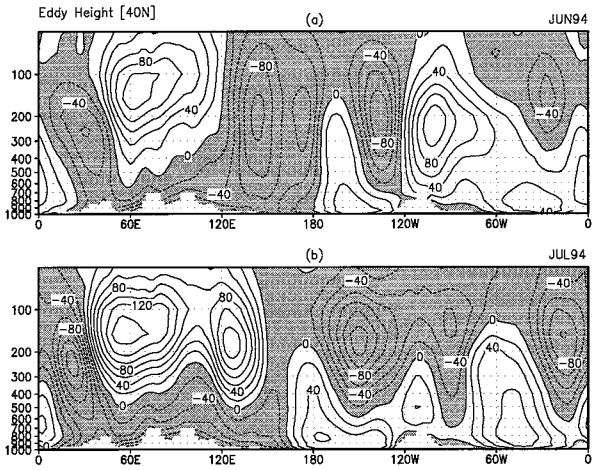

FIG. 5. Same as Fig. 2 but for (a) June and (b) July 1994.

The Northern Hemispheric SST tendency (Figs. 4d–f) reflects a delayed response of the ocean surface thermal field to the insolation with about a two-month lag. Positive SST tendencies occur throughout the North Pacific and the North Atlantic between June and August (Figs. 4d–e), while weak negative tendencies occur between August and September. The July to August tendency (Fig. 4e) shows the largest positive SST changes over the North Pacific and off the east coast of North America. The local maxima in SST tendencies tend to be located just south and slightly east of the maxima in the height tendencies in the regions of strong positive height gradients.

The above results show that while there is a strong zonal mean component to the seasonal changes in the warm season circulation, there are, not surprisingly, also substantial zonal asymmetries that suggest zonally asymmetric forcing. Over Asia, the enhanced height tendencies near 40°N between June and July presumably reflect the heating from the warm interior Asian land surface. We shall see in the next section that this is linked to a substantial shift in the zonal wind over this region and changes in the orographic forcing. Throughout the summer, the patterns of the height tendency and the underlying ocean surface warming suggest a strong coupling between the atmosphere and ocean, though the nature of this coupling is not clear. Before pursuing these questions further, we look next at the 1994 summer anomalies and how they relate to the climatological features described above.

b. The 1994 anomalies

In June 1994, the stationary wave pattern (Fig. 5) is characterized by midocean troughs and upper-level ridges over the continents, which is similar to the June climatology in Fig. 2a. However, a substantial difference

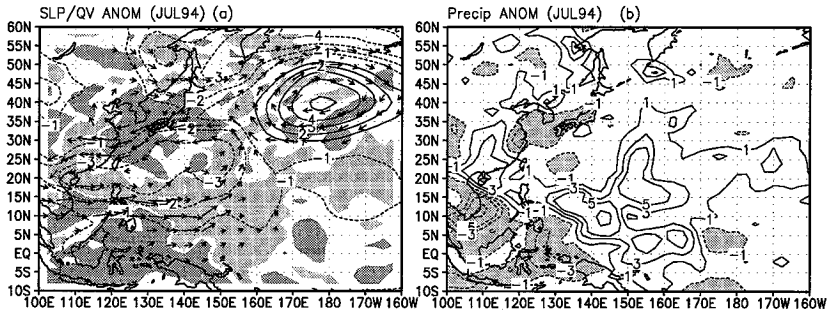

FIG. 6. The July 1994 anomalies for (a) sea level pressure (contoured), vertically integrated moisture flux (vectors), moisture convergence (shading), and (b) precipitation. In (a), contour interval is 1 mb. The vectors are in the unit of g kg^{-1} m s^{-1} with arbitrary size. Darker shading represents the values less than -1 mm day^{-1} and lighter shading represents the values greater than 1 mm day^{-1}. In (b), contours are drawn at -10, -5, -3, -1, 1, 3, 5, and 10 mm day^{-1}. Shading represents the values less than -1 mm day^{-1}.

is found between the July 1994 upper-level stationary waves and the July climatology. The stationary wave pattern during July 1994 is characterized by a much pronounced ridge over the East Asia–western Pacific region and deeper midocean troughs over the eastern Pacific and the Atlantic, and a much weaker continental high over North America: these resemble the August climatology (Fig. 2c). The August-like circulation anomalies during July 1994 suggest an unusual seasonal evolution of the middle latitude stationary waves. The seasonal cycle appears to jump from June to August conditions and skip the normal July circulation, which is crucial for the monsoon rainfall over East Asia.

The Pacific high is substantially intensified over the central North Pacific during July 1994, while a belt of lower pressure is found over the western Pacific off the east coast of south China (Fig. 6a). The northward moisture transport over the North Pacific is shifted eastward (consistent with the intensified subtropical high) resulting in a substantial reduction of the usual moisture supply to East Asian–western Pacific region from the southern flank of the climatological subtropical high. In the subtropics, the cyclonic circulation anomalies associated with lower pressure over the western Pacific are responsible for the reduced moisture supply from the Indian monsoon region. These circulation changes are responsible for the reduced moisture convergence (darker shading) over East Asia. Moisture is transported instead toward the central Pacific to enhance the moisture convergence (lighter shading) over a large region east of 130°E (Fig. 6a).

In Fig. 6b, dry conditions associated with the reduced moisture supply are found over the tropical western Pacific, and over the large region in the middle latitudes extending from central China to the southern parts of Korea and Japan, while wet conditions are found over the subtropical Pacific. These anomaly patterns of moisture convergence and rainfall from the assimilation are relatively consistent in the middle latitudes as well. Particularly, the substantially reduced rainfall and moisture convergence over the southern parts of central China, Korea, and Japan are well represented, suggesting that the assimilation provides useful information about the rainfall in this region when the systematic bias is effectively removed (see also Schubert et al. 1995).

The anomalies in Figs. 6a and 6b bear some resemblance to the climatological tendency patterns in Figs. 3c and 3d, respectively. Substantial differences are found, however, in the pressure patterns (Figs. 3c and 6a) over central China and the central North Pacific. In Fig. 6b, the C-shaped region of drier conditions around the coastal lines and islands, with wetter conditions near the center over the central Pacific are almost identical to the climatological July to August tendencies in Fig. 3d except for a slight latitudinal displacement.

Figure 7 shows the 200-mb height, SST, and thickness anomalies for July 1994. The upper-level circulation anomalies during July 1994 (Fig. 7a) are dominated by a persistent stationary wave pattern in the middle latitudes with pronounced positive height anomalies over East Asia, western North America, the Canadian Maritime Provinces, and Scandinavia. These unusually persistent positive height anomalies were blamed for the record-breaking summer heat waves and drought conditions over East Asia and northern Europe (Climate Analysis Center 1994). Figure 7b shows that the atmospheric anomalies are accompanied by positive SST anomalies in the Tropics and middle latitudes, and weak negative anomalies in the subtropics. The middle latitude positive SST anomalies are most pronounced in the central North Pacific and off the east coasts of both continents. We note that the June SST anomalies (not shown) are similar to the July values in the Tropics and subtropics, but the central North Pacific positive anomalies are absent, indicating the latter developed rather quickly. Figures 7c and 7d, show the thickness anomalies in the upper troposphere (between 200 and 600 mb) and in the lower troposphere (between surface and 600 mb), representing the mean temperature anomalies within these layers for July 1994. These figures show

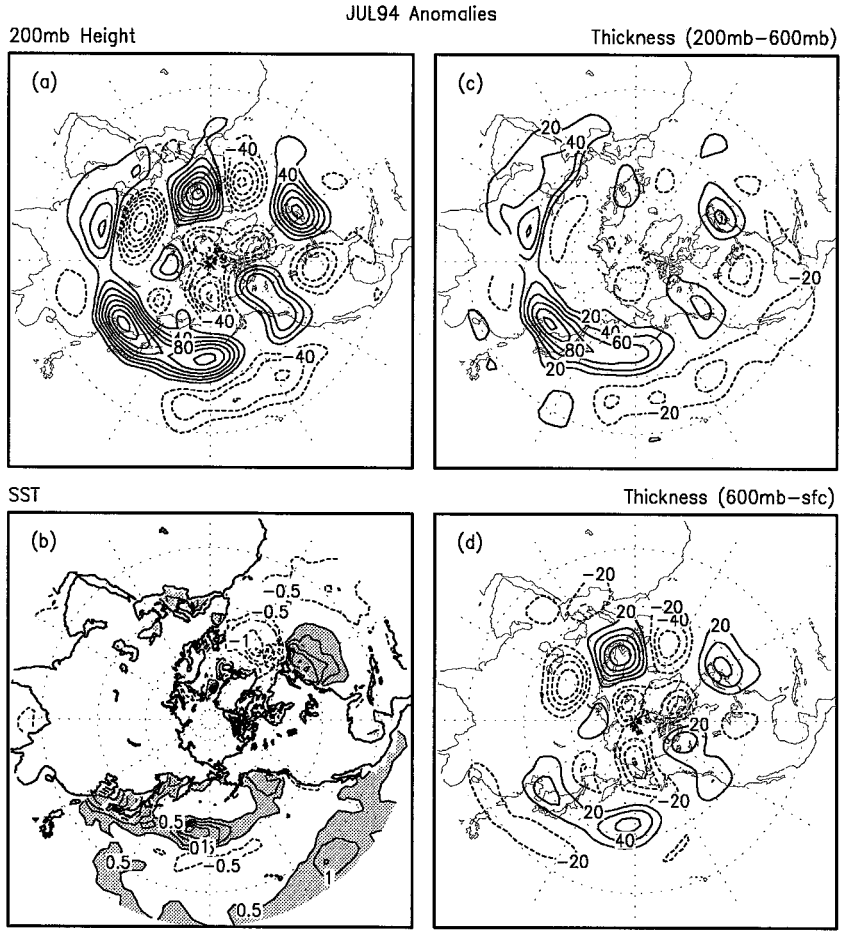

FIG. 7. (a) The 200-mb height and (b) SST anomalies for July 1994. Contour interval is 20 m in (a) and 0.5°C in (b). The zero contours are not drawn. Shading represents positive anomalies greater than 0.5°C in (b). Dotted lines represent the negative values. The thickness anomalies for July 1994 in (c) the upper troposphere (200 mb–600 mb) and (d) the lower troposphere (600-mb surface). Contour interval is 20 m.

that there are large differences in the vertical structure of the Eurasian and East Asian anomaly patterns with the temperature anomaly signal over northern Europe almost entirely confined to the lower troposphere while the East Asian anomaly is primarily an upper-level signal. The upper-tropospheric anomalies are characterized by barotropic and equivalent barotropic structure over northern Europe and East Asia, respectively. The east coast and central North Pacific lower-tropospheric positive thickness anomalies appear to be linked to the underlying local SST anomalies (Figs. 7b and 7d). The strong upper-tropospheric thickness anomaly over the East Asian region suggests that this anomaly is driven primarily by upper-level dynamics and that local SST forcing may be of secondary importance. The nature of the strong lower-tropospheric waves extending across northern Europe into Asia is not clear (see, however, discussion in section 5).

In the context of the broader scale Asian monsoon, we note that the Indian monsoon was near normal in July 1994, except for some localized wet conditions over northern India and Pakistan (Climate Analysis Center 1994). Figure 8a does show a region of weak convergence over India and a more substantial signal in the upper-level divergence over the western Pacific just north of the equator. The moisture flux convergence and precipitation anomaly patterns in Fig. 6 suggest, however, that the upper-level divergence anomalies over the western Pacific may be the result of the enhanced convection associated with anomalous moisture convergence over that region due to the circulation changes in middle latitudes. The streamfunction anomalies in Fig. 8b also show that the middle latitude anomalies have no obvious connection to the Tropics: the most pronounced tropical divergence anomalies are located downstream of the middle latitude anomalies. In the next section, we focus on possible forcing mechanisms outside the Tropics.

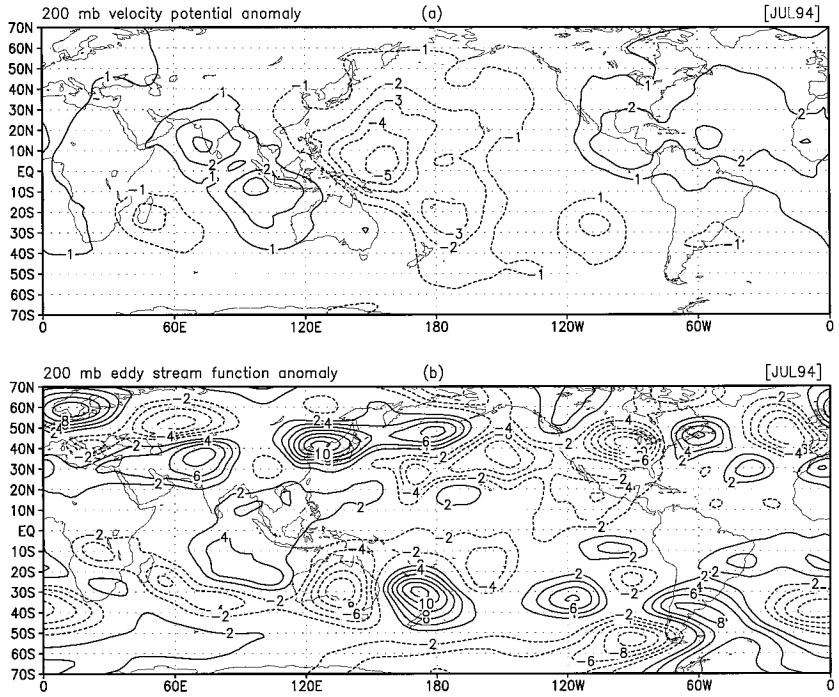

FIG. 8. (a) The 200-mb velocity potential and (b) eddy streamfunction anomalies for July 1994. Contour intervals are 1.0×10^6 m^2 s^{-1} in (a) and 2.0×10^6 m^2 s^{-1} in (b). Dotted lines represent the negative values.

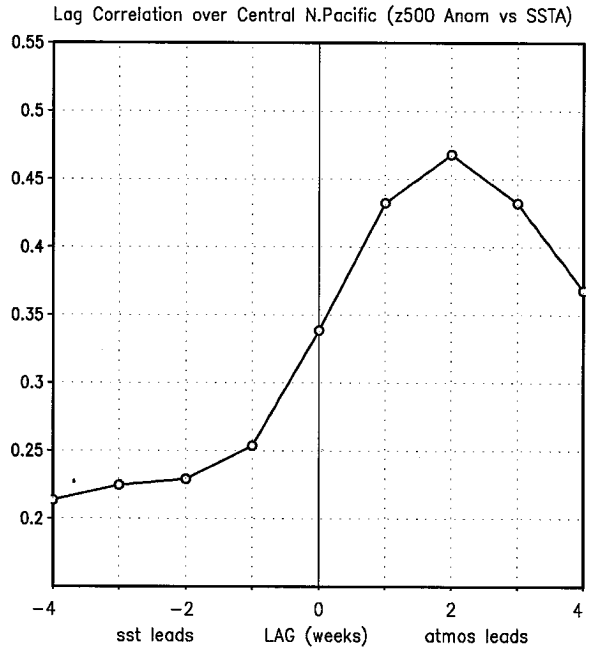

FIG. 9. Lag correlation between the SST and 500-mb height anomalies during the warm season (May–September) over the central North Pacific (35°–45°N, 150°E–150°W). The abscissa represents the lag between the two time series in weeks; positive when height leads SST.

3. Forcing mechanisms

While the above results suggest an SST connection to the stationary wave anomalies in the middle latitudes, the forcing mechanism actually responsible for the development of the East Asian anticyclonic anomalies is not clear. The equivalent barotropic structure of the stationary waves over East Asia indicates that the local warming of the middle latitude SSTs over the coastal regions of East Asia and northwestern Pacific is not likely the direct cause of the persistent anomaly over East Asia. As discussed by Frankignoul (1985) in his comprehensive review of air–sea feedback processes in the midlatitudes, numerous observational and modeling studies suggest that middle latitude SST anomalies are ineffective at generating circulation anomalies. On the other hand, Webster (1981) shows, with a linear model, that the weaker summer zonal wind may allow a stronger response to middle latitude SSTs. To examine this possibility we show in Fig. 9 the time-lagged correlations between the weekly SST anomalies over the central North Pacific and 500-mb height anomalies for the warm season. The results show that the atmospheric anomalies are leading the SST anomalies by about 2 weeks. Thus, it appears unlikely that the SST anomalies are initiating the atmospheric anomalies, though we have not ruled out the possibility that the SST anomalies, once established, are feeding back on the circulation. The nonzero correlation at zero lag may in fact suggest this is the case. As already mentioned, the trop-

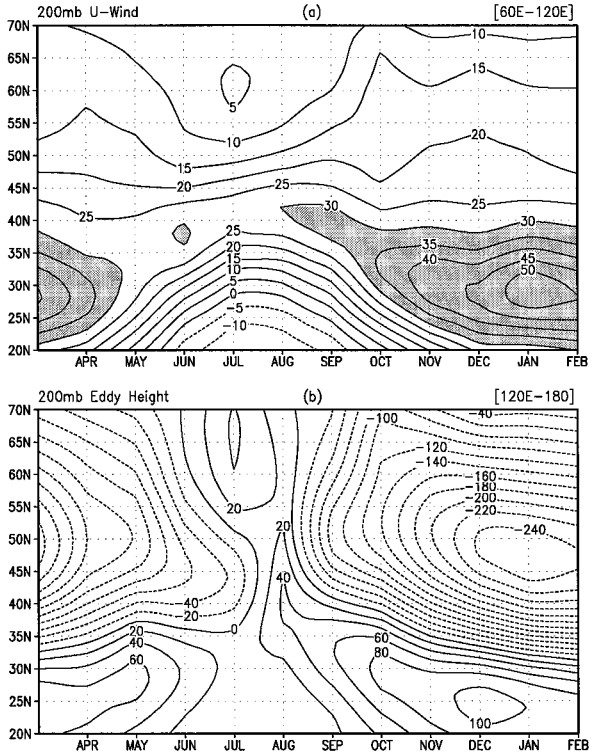

FIG. 10. Latitude–time evolution of the climatological seasonal cycle of (a) the 200-mb u-wind averaged over the Asian–Pacific sector (60°–120°E) and (b) the 200-mb eddy height averaged over the western Pacific region (120°E–180°). Contour intervals are 5 m s^{-1} for the zonal wind and 20 m for the height. Dotted lines represent the negative values. The values greater than 30 m s^{-1} are shaded in (a).

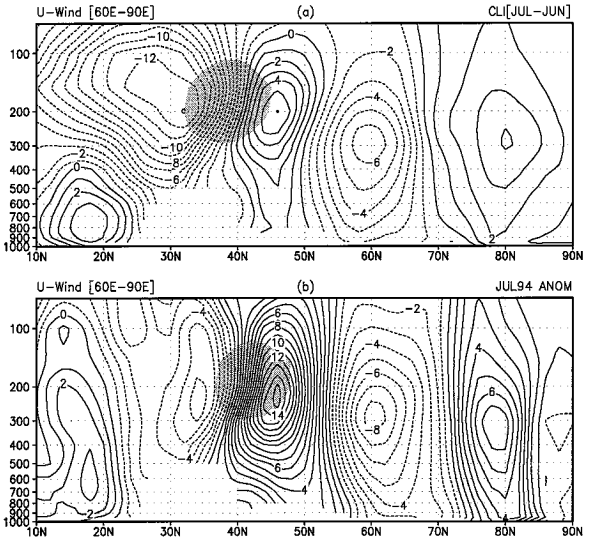

FIG. 11. The latitude-pressure sections of the u-wind for (a) the climatology difference (July–June) and (b) July 1994 anomaly. Shading represents the u-wind greater than 20 m s^{-1} for June climatology in (a) and July climatology in (b). The values are averaged over the western mountain terrain (60°–90°E). Contour interval is 1 m s^{-1}.

ical SST anomalies are weak and changed little between June and August of 1994, and thus also appear unlikely to be the cause of the east Asian anticyclonic anomaly.

Next we consider the possibility that orographic forcing is playing a role. Figure 10a shows the seasonal evolution of the 200-mb zonal wind averaged over the high mountain terrain between 60°E and 120°E. The most pronounced change is the weakening and northward movement of the strongest winds during the summer season. The period between June and July, in particular, is marked by a rapid northward shift of the jet between 30° and 40°N latitude, suggesting substantial changes in the orographic forcing in this region. This is followed by near steady zonal wind in July. These changes in the zonal wind are accompanied by major reductions in the strength of the east Asian trough such that by late July the eddy height field becomes positive (Fig. 10b), reflecting the east Asian anticyclone discussed earlier.

The cross section of the June to July zonal wind changes are shown in Fig. 11a, where we have now focused on the changes over the western Tibetan Plateau (60–90°E) to avoid any influences from the ''response'' of the East Asian anticyclone. This shows clearly the northward shift of the jet with much weakened winds over the highest terrain and strengthened winds on the northern slopes. The July 1994 anomaly in the zonal wind for the same region is shown in Fig. 11b. The anomalies indicate that 1994 experienced zonal wind anomalies similar in structure to the climatological change but much enhanced in amplitude. This shift in the jet is evidently produced by the anomalous and persistent 1994 Eurasian waves extending into this region as seen from Fig. 7a. Thus, both the climatological and anomalous changes in the zonal wind over Tibet likely have a similar impact on the orographic forcing.

The propagation and sources of wave activity may be studied in terms of the wave activity vectors as defined by Plumb (1985), which is an extension of the Eliassen–Palm relation (Edmon et al. 1980) to three dimensions. The flux components, which are applicable for quasigeostrophic stationary waves on a zonal flow, are

$$F_{\lambda} = \frac{p}{2000a^2 \cos\phi}\left[\left(\frac{\partial\Psi'}{\partial\lambda}\right)^2 - \Psi'\frac{\partial^2\Psi'}{\partial\lambda^2}\right] \quad (1a)$$

$$F_{\phi} = \frac{p}{2000a^2}\left(\frac{\partial\Psi'}{\partial\lambda}\frac{\partial\Psi'}{\partial\phi} - \Psi'\frac{\partial^2\Psi'}{\partial\lambda\partial\phi}\right) \quad (1b)$$

and

$$F_z = \frac{p\Omega^2 \sin^2\phi}{500N^2 a}\left(\frac{\partial\Psi'}{\partial\lambda}\frac{\partial\Psi'}{\partial z} - \Psi'\frac{\partial^2\Psi'}{\partial\lambda\partial z}\right), \quad (1c)$$

where

$$N^2 = \left(\frac{Rp^{\kappa}}{H}\right)\frac{\partial\Theta}{\partial z}.$$

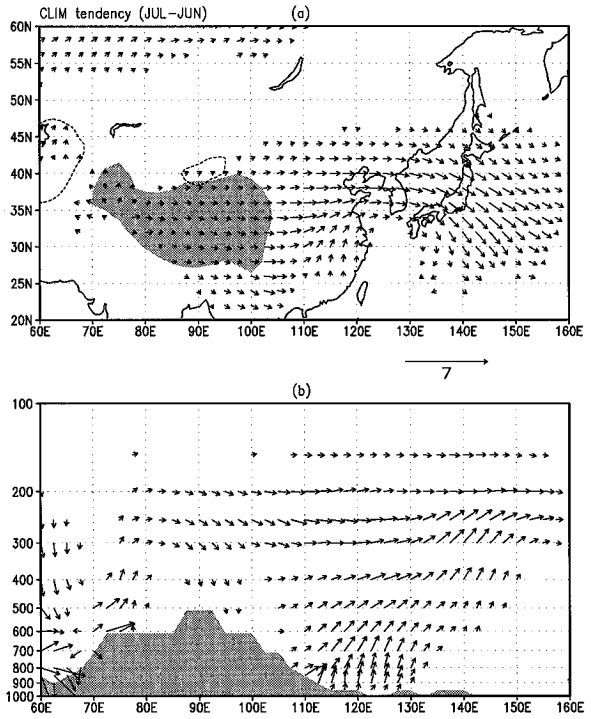

FIG. 12. (a) The wave activity fluxes based on the streamfunction for the climatology difference (July–June). Contours represent the vertical component at the 300-mb level and vectors represent the horizontal component of wave activity flux at the 200-mb level. A reference vector of 7 $m^2\ s^{-2}$ is shown at the bottom. Contour interval is $2.0–10^{-3}\ m^2\ s^{-2}$. The zero contours are not drawn. Shading represents the topography at the 700-mb level. (b) The longitude-pressure sections of the wave activity fluxes averaged between 30° and 40°N. The vector size is arbitrary.

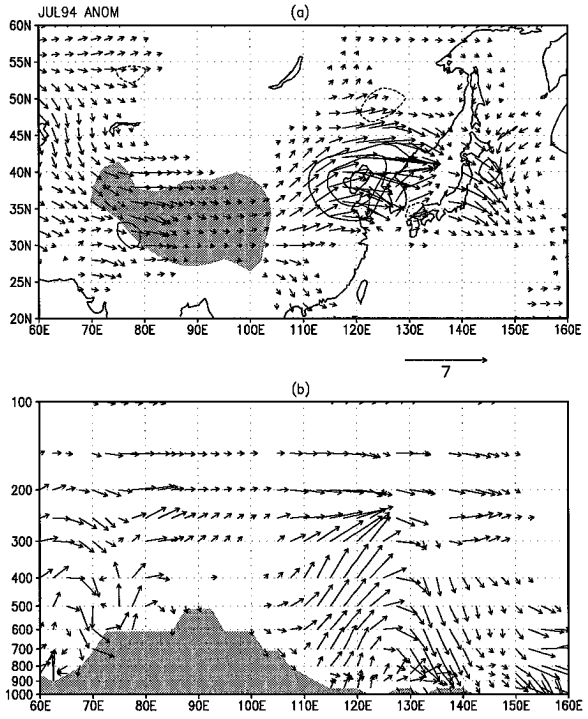

FIG. 13. Same as Fig. 12 but for July 1994 anomalies.

Here, Θ is the zonally averaged potential temperature, $z = -H \ln p$, and H is a constant scale height. Also, Ψ' is the eddy streamfunction (deviation from zonal mean), p is pressure, ϕ is latitude, λ is longitude, and a is the radius of the earth. Of particular interest in using this diagnostic is to determine the impact of the local or upstream wave sources on the development of the East Asian anticyclone east of the Himalayas. The reader is also referred to Karoly et al. (1989) for further examples of the use of this diagnostic.

The wave activity flux vectors for the climatological July minus June stationary waves treated as anomalies are shown in Fig. 12. The horizontal fluxes (Fig. 12a) appear to emanate from the region of Tibet where they are directed eastward across the east coast and then turn toward the equator. The vertical and meridional components of the flux (12b) show that the flux appears to emanate somewhat downstream of the orography. Such a phase shift with respect to the orography was also noted in an idealized study of this wave activity flux diagnostic (Plumb 1985), suggesting the current results are not inconsistent with an orographic forcing of the waves.

The wave activity flux vectors for the anomalous stationary waves during July 1994 are shown in Fig. 13. The horizontal wave activity fluxes (Fig. 13a) show fluxes of wave activity over the Eurasian continent directed toward Tibet. Another stream of wave activity emanates from the eastern slopes of the Tibetan Plateau, suggesting an enhancement of the climatological flux shown in Fig. 12a. This is accompanied by pronounced vertical fluxes, again, phase shifted with respect to the highest mountains. Figure 13b shows the longitude-pressure sections of the wave activity flux anomalies. This view of the fluxes shows the apparent source is confined to the East Asian region with upward fluxes and enhanced zonal propagation east of Tibet and the downward fluxes around Japan. The enhanced zonal propagation in the upper troposphere is clearly tied to the enhanced vertical fluxes on the eastern slope of the Tibetan Plateau. We note that the total diabatic heating anomalies over those regions (not shown) appear to be too weak to force the anomalous wave activity fluxes.

These results suggest that the changes in forcing associated with orography are largely responsible for both the seasonal and anomalous development of the East Asian anticyclone, though, as mentioned earlier, it is not unlikely that the continued development of the East Asian anticyclone is reinforced by feedbacks from the underlying ocean surface (see Figs. 4e and 7b).

The thickness patterns (Fig. 7) and the wave activity flux vectors (Fig. 13) suggest that the European waves and the east Asian anticyclone are effectively decoupled, or at least they are not directly related events. It is suggested, however, that the Eurasian wave pattern indi-

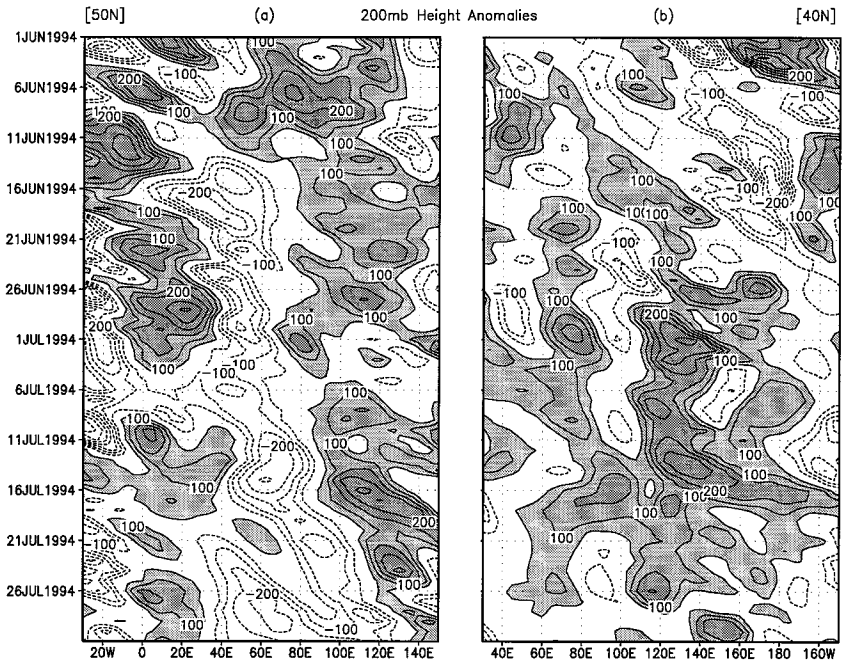

FIG. 14. Longitude-time evolution of the 200-mb height anomalies at (a) 50°N and (b) 40°N. Contour interval is 50 m. The zero contours are not drawn. Shading represents positive anomalies greater than 50 m. Dotted lines represent the negative values.

rectly influences the East Asian anomalies by changing the circulation around Tibet, which causes a change in the forcing due to orography. The relative timing of these two events is shown in Fig. 14, which compares the evolution of the 200-mb height anomalies at 50°N (Fig. 14a, capturing the Eurasian waves) and 40°N (Fig. 14b, capturing the east Asian anticyclone). The beginning of the wave pattern over northern Europe is already evident in early June. By mid-June a strong stationary component with positive anomalies west of 20°E and negative anomalies to the east is firmly established (Fig. 14a). On the other hand, the persistent positive anomaly over East Asia does not begin to develop until the middle of June (Fig. 14b). The anomaly development starts on the west side of the mountains. It is not until late June that the positive anomaly to the east of Tibet intensifies rapidly. The East Asian anomaly remained near 130°E for about 40 days with little break during that time. We note that while the persistent anomaly at 130°E is predominantly a standing feature, there is also a substantial eastward propagating signal that develops in mid-July.

4. Interannual variability

In this section we examine the entire 9-yr record available from the GEOS-1 assimilation to determine how the 1994 East Asian summer anomalies compare with previous years. The underlying hypothesis is that the 1994 anomalies are an extreme example of fluctuations in the seasonal cycle that occur on a more frequent basis. We focus on the zonal wind fluctuations and use an empirical orthogonal function (EOF) analysis to provide an index of the circulation variability.

Figure 15a shows the dominant EOF of the July and August zonal wind averaged for the sector 90°E–120°W longitude for the years 1985–93. This mode accounts for 45% of the variance. Figure 15b shows the evolution of the first zonal wind EOF during July and August for 1985–93. The July value for 1994 is the projection of the 1994 wind anomaly onto the EOF computed from the previous nine years (the assimilation has currently been run only to the end of July 1994). The variation occurs at low frequency with positive values occurring prior to 1986, between 1988 and 1991, and again in 1994. Figure 15c shows the variation of SST anomalies over the central North Pacific (35°–45°N, 150°E–150°W) for the same time period. The correspondence with the zonal wind variation is quite remarkable, suggesting a strong link between zonal wind changes and SSTs. For example, the large negative zonal wind anomaly index is consistent with cold SST anomalies in the middle latitude Pacific in 1987 and 1993, and the large positive zonal wind anomaly index with warm SST anomalies in 1990 and 1994.

The composite difference of the height and SST field between pronounced positive and negative years (for 1985–93 based on the first zonal wind EOF) is shown in Fig. 16. The anomaly structures are similar to those of 1994, with a pronounced area of enhanced heights extending off the east coast of Asia, and wave pattern extending across North America, Europe, and Asia (Fig.

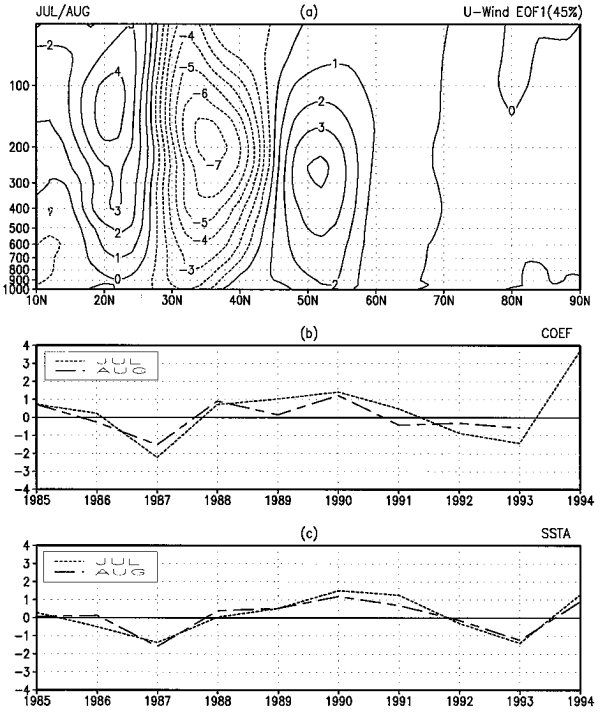

FIG. 15. (a) The first EOF pattern of u-wind averaged in the East Asian–Pacific sector (90°E–150°W), (b) its corresponding coefficients, and (c) SST anomalies over the central North Pacific (35°–45°N, 150°E–150°W). Units are in degree in (c).

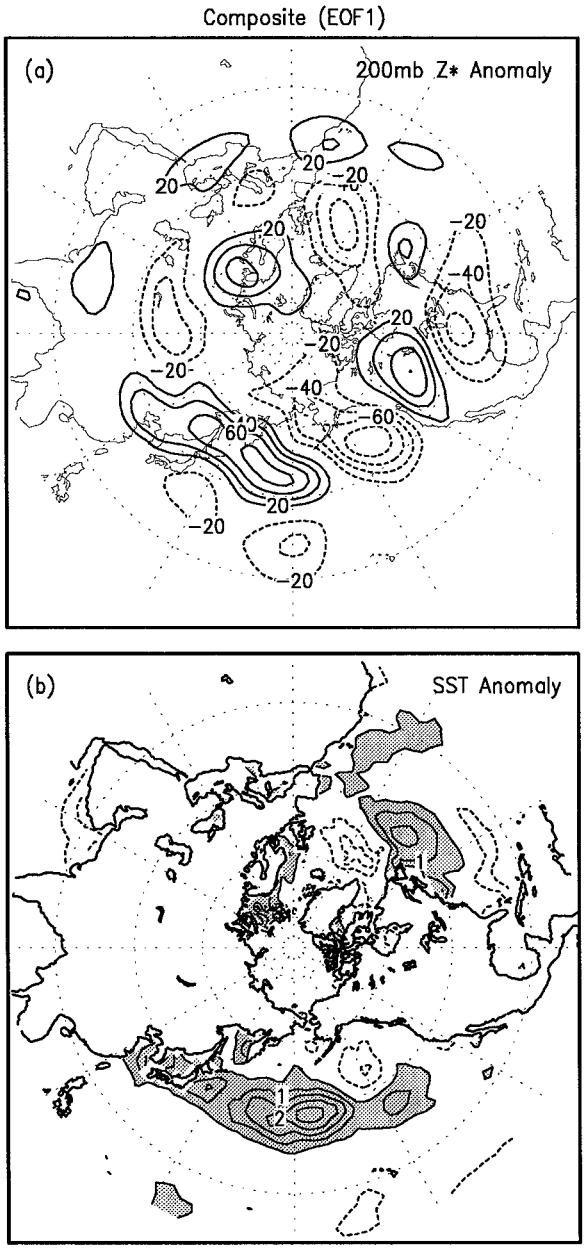

FIG. 16. (a) The 200-mb eddy height and (b) SST anomalies for the composite difference, represented as high minus low, based on the coefficients in Fig. 15b. Contour interval is 20 m in (a) and 0.5°C in (b). The zero contours are not drawn. Shading represents positive anomalies greater than 0.5°C in (b). Dotted lines represent the negative values.

7a), while some difference is found over the Gulf of Alaska with a deeper trough in the composite. Figure 16b shows that positive SST anomalies are most pronounced over the central North Pacific and over the northwestern North Atlantic off the east coast of Canada. The similarity to the July 1994 middle latitude SST anomalies (Fig. 7b) is remarkable, while major differences are found in the tropical Pacific, suggesting that the middle latitude waves are not connected with tropical SST forcing.

Figure 17 shows the accumulated summer (July and August) precipitation over Korea (obtained from the Korea Meteorological Administration) averaged over 14 stations for each of the ten years (1985–94). The interannual variation of the Korean rainfall has a clear quasi-biennial oscillation with alternating dry and wet conditions. Comparison of the Korean rainfall variations with those of the leading mode of the u-wind (Fig. 15b) shows an apparent linkage: the wet years (1987, 1991, and 1993) correspond to negative index years, while the dry years (1988, 1990, and 1994) correspond to positive index years. This further supports the idea that the East Asian monsoon is strongly tied to the zonal wind variations over the Tibetan Plateau.

5. Discussion and conclusions

This study documents and analyzes the unusual evolution of the East Asian circulation during the summer of 1994. The results show that the abnormal evolution of the seasonal cycle, which is associated with the early development of the upper-level anticyclonic flow over East Asia, is responsible for the absence of the middle latitude monsoon rainfall (Changma in Korea and Baiu in Japan) during July. The July circulation anomalies associated with the development of the anticyclone east of the Himalayas and the cyclonic circulation off the

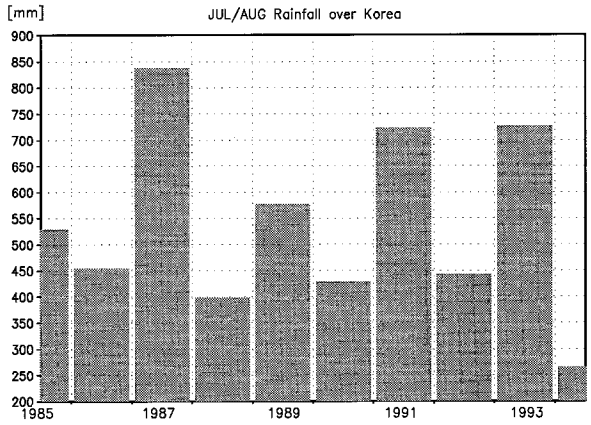

FIG. 17. Accumulated precipitation for July and August over Korea. Units are in mm.

east coast of south China, which are more typical of the August climatology, acted to suppress the moisture supply from the Indian Ocean and the southern flank of the subtropical high leading to suppressed rainfall over the southern parts of Korea and Japan.

The circulation anomalies are strongly linked with SST anomalies in the middle latitudes. Lag correlations suggest, however, that the atmosphere is driving the ocean changes with a time lag of about two weeks. This result is similar to what has been found for the cold season in several previous studies. In particular, Wallace and Jiang (1987) found that circulation anomalies lead SST anomalies over the central North Pacific by about a month. Tropical Pacific SST anomalies are considerably weaker than the middle latitude SST anomalies during 1994 and change little between June and July, suggesting they play little role in the development of the east Asian drought.

This study has attempted to find a common forcing that explains the development of 1994 East Asian anomalies, those which occurred in previous years (with similar structure), as well as the climatological development of the east Asian anticyclone. It is shown that the July circulation anomalies and associated fluxes of wave activity are consistent with an enhancement of the climatological orographic forcing during that month. This is associated with a northward shift in the jet over Tibet, which leads to weakened westerlies over the high terrain (with strengthened westerlies to the north). This shift is an enhancement of the radiatively driven seasonal change that typically occurs during that month. During anomalous years, and during 1994 in particular, the change in the zonal wind occurs as a result of anomalous Eurasian wave trains, which impinge on the Tibetan Plateau. It is suggested that the enhancement of the typical late June and July orographic forcing is the primary cause of the premature development of the 1994 east Asian anticyclone, which, by circumventing the normal July rainy season, leads to the east Asian drought. An inspection of the previous nine summers showed that anomalies similar in structure to the 1994 pattern have occurred in other years (though not as strong). These anomalies tied to the orographic forcing appear to be crucial for the summer monsoon rainfall over East Asia.

The role of orography in the development of the stationary waves east of the mountains has been investigated in a number of studies using diagnostic models (e.g., Hoskins and Karoly 1981; Blackmon et al. 1987; Chen and Trenberth 1988; Nigam et al. 1988; Valdes and Hoskins 1989; Kang 1990; Ting 1994). Chen and Trenberth, in particular, examined the orographic effect of the total flow including contributions from the basic state and wave flows during northern winter. They found that thermally induced orographic forcing is necessary to successfully reproduce the observed stationary waves. In the present case, the orographic forcing is believed to be the result of the interaction with the anomalous Eurasian waves extending into central Asia. This is consistent with the study by Ting (1994), which showed that, while the linear orographic response is weak during summer, the nonlinear interaction between the thermally driven circulation and local orography may play a significant role in determining the summertime stationary waves in the extratropics.

A number of issues remain unresolved. For example, the causes of the wave pattern over the Eurasian continent are unclear. The fact that similar anomalies have occurred in previous years suggests this may be a natural mode of the summer circulation. Several recent studies have pointed out the potentially important role of preceding middle latitude anomalies in the development of the monsoon. For example, Yasunari and Seki (1992) and Meehl (1994) suggested that the summertime monsoon is strongly coupled with ENSO in which preceding oceanic and atmospheric conditions set up middle latitude anomalies, which impact subsequent monsoon development. Another issue concerns the exact nature of the interaction between the zonal wind anomalies and the orography. This can be addressed only with additional studies employing realistic linear and nonlinear atmospheric models. The zonal wind anomalies may influence the stationary waves in other ways as well. For example, Nigam and Lindzen (1989) show that the propagation of the middle latitude stationary waves is sensitive to the small shifts in the position of the East Asian jet by opening or closing the path for propagation on the equatorward side of the jet. Besides a connection with the Eurasian wave pattern, there are other mechanisms for modifying the zonal wind. Changes in the Tropics, for example, can influence the strength and position of the Tibetan high. As White (1982) suggested, some aspects of the middle latitude stationary waves over the Eurasian continent might be a remote response to the monsoon circulation interacting with high mountains in early summer. Finally, the implications for monsoon prediction are obvious, although the role of Tropics has yet to be clarified. If the proposed mechanism is

correct, it becomes imperative that we focus on understanding and predicting the Eurasian wave pattern, and its interaction with the Tibetan Plateau.

Acknowledgments. We wish to thank C.-H. Ho, who provided Korean precipitation data. We also would like to thank two anonymous reviewers. Their comments resulted in significant improvements to the manuscript. This work was supported by the Global Atmospheric Modeling and Analysis Program, Office of Mission to Planet Earth, NASA Headquarters.

APPENDIX

The Data Assimilation Office (DAO) at the NASA Goddard Space Flight Center has recently produced a multiyear global dataset (Schubert et al. 1993) and a special dataset for the summer of 1994, employing a fixed assimilation system. The main components of the GEOS1 (version 1) data assimilation system (DAS) are the GEOS–DAS atmospheric general circulation model (Takacs et al. 1994; Suarez and Takacs 1995) and a three-dimensional, multivariate optimal interpolation (OI) scheme (Pfaendtner et al. 1995). The GEOS-1 DAS is summarized below.

The OI analysis scheme is carried out at a horizontal resolution of 2° lat × 2.5° long at 14 upper-air pressure levels and at sea level. The analysis increments are computed every 6 h using observations from a ±3-h data window centered on the analysis times. For the global sea level pressure and near-surface wind analysis over the oceans, data from surface land synoptic reports (sea level pressure only), ships, and buoys are used. The upper-air analyses of height, wind, and moisture incorporate the data from rawinsondes, dropwindsondes, rocketsondes, aircraft winds, cloud-tracked winds, and thicknesses from the historical TOVS soundings produced by NOAA NESDIS. The assimilation system does not include an initialization scheme and relies on the damping properties of a Matsuno time-differencing scheme to control initial imbalances generated by the insertion of observations. However, the initial imbalances and spinup have been greatly reduced over earlier versions by the introduction of an incremental analysis update (IAU) procedure (Bloom et al. 1991).

The GEOS-1 GCM uses the potential enstrophy and energy-conserving horizontal differencing scheme on a C-grid developed by Sadourny (1975). The model's vertical finite differencing scheme is that of Arakawa and Suarez (1983). The dynamics routines are organized into a plug-compatible module developed by Suarez and Takacs (1995).

The infrared and solar radiation parameterizations follow closely those described by Harshvardhan et al. (1987). The penetrative convection originating in the boundary layer is parameterized using the Relaxed Arakawa–Schubert (RAS) scheme (Moorthi and Suarez 1992), which is a simple and efficient implementation of the Arakawa–Schubert (1974) scheme. The planetary boundary layer is explicitly resolved in a 2–4 layer region. Wind, temperature, and humidity profiles in an ''extended'' surface layer, and the turbulent fluxes of heat, moisture, and momentum at the surface are obtained from Monin–Obukov similarity theory. Turbulent fluxes above the ''extended'' surfaced layer are computed using the second-order closure model of Helfand and Labraga (1988). The GEOS-1 GCM is run without a land surface model. For the assimilation described here, the soil moisture is computed off-line based on a simple bucket model using climatological surface air temperature and precipitation (Schemm et al. 1992). The snow line and surface albedo are prescribed and vary with the season. The sea surface temperature is updated according to the observed monthly mean values provided by the Climate Analysis Center at the National Meteorological Center (now known as the National Centers for Environmental Prediction) and the Center for Ocean, Land and Atmosphere (COLA), Calverton, Maryland.

REFERENCES

Arakawa, A., and W. Schubert, 1974: Interaction of a cumulus cloud ensemble with the large-scale environment. Part I. *J. Atmos. Sci.,* **31,** 674–701.

——, and M. J. Suarez, 1983: Vertical differencing of the primitive equations in sigma coordinates. *Mon. Wea. Rev.,* **111,** 34–45.

Blackmon, M. L., G. W. Branstator, and G. T. Bates, 1987: An analysis of equatorial Pacific sea surface temperature anomaly experiments in general circulation models with and without mountains. *J. Atmos. Sci.,* **44,** 1828–1844.

Bloom, S. C., L. L. Takacs, and E. Brin, 1991: A scheme to incorporate analysis increments gradually in the GLA assimilation system. Preprints, *Ninth Conf. on Numerical Weather Prediction,* Denver, CO, Amer. Meteor. Soc., 110–112.

Broccoli, A. J., and S. Manabe, 1992: The effects of orography on midlatitude Northern Hemisphere dry climates. *J. Climate,* **5,** 1181–1201.

Chen, S.-C., and K. E. Trenberth, 1988: Forced planetary waves in the Northern Hemisphere winter: Wave coupled orographic and thermal forcings. *J. Atmos. Sci.,* **45,** 682–704.

Climate Analysis Center, 1994: Near real-time analyses ocean/atmosphere. *Climate Diagnostic Bulletin,* **94/7,** 63–74.

Ding, Y., 1994: *Monsoons over China.* Kluwer Academic Publishers, 419 pp.

Edmon, H. J., B. J. Hoskins, and M. E. McIntyre, 1980: Eliassen–Palm cross-sections for the troposphere. *J. Atmos. Sci.,* **37,** 2600–2616.

Frankignoul, C., 1985: Sea surface temperature anomalies, planetary waves, and air–sea feedback in the middle latitudes. *Rev. Geophys.,* **23,** 357–390.

Hahn, D. J., and S. Manabe, 1975: The role of mountains in the South Asian monsoon circulation. *J. Atmos. Sci.,* **32,** 1515–1541.

Harshvardhan, R. Davies, D. A. Randall, and T. G. Corsetti, 1987: A fast radiation parameterization for atmospheric circulation models. *J. Geophys. Res.,* **92,** 1009–1016.

Helfand, H. M., and J. C. Labraga, 1988: Design of a non-singular level 2.5 second-order closure model for the prediction of atmospheric turbulence. *J. Atmos. Sci.,* **45,** 113–132.

Hoskins, B. J., and D. J. Karoly, 1981: The steady linear response of a spherical atmosphere in thermal and orographic forcing. *J. Atmos. Sci.,* **38,** 1179–1196.

Kang, I.-S., 1990: Influence of zonal mean flow change on stationary wave fluctuations. *J. Atmos. Sci.,* **47,** 141–147.

Karoly, D. J., R. A. Plumb, and M. Ting, 1989: Examples of the horizontal propagation of quasi-stationary waves. *J. Atmos. Sci.,* **46,** 2802–2811.

Meehl, G. A., 1994: Coupled land–ocean–atmosphere processes and South Asian monsoon variability. *Science,* **266,** 263–267.

Molod, A., H. M. Helfand, and L. L. Takacs, 1996: The climatology of parameterized physical processes in the GEOS-1 GCM and their impact on the GEOS-1 data assimilation system. *J. Climate,* **9,** 764–785.

Moorthi, S., and M. J. Suarez, 1992: Relaxed Arakawa–Schubert: A parameterization of moist convection for general circulation models. *Mon. Wea. Rev.,* **120,** 978–1002.

Murakami, T., 1987: Effects of the Tibetan Plateau. *Monsoon Meteorology*. C.-P. Chang and T. N. Krishnamurti, Eds., Oxford University Press, 235–270.

Nigam, S., 1994: On the dynamical basis for the Asian summer monsoon rainfall–El Niño relationship. *J. Climate,* **7,** 1750–1771.

——, and R. S. Lindzen, 1989: The sensitivity of stationary waves to variations in the basic state zonal flow. *J. Atmos. Sci.,* **46,** 1746–1768.

——, I. M. Held, and S. W. Lyons, 1988: Linear simulation of the stationary eddies in a GCM. Part II: The ''mountain'' model. *J. Atmos. Sci.,* **45,** 1433–1452.

Pfaendtner, J., S. Bloom, D. Lamich, M. Seablom, M. Sienkiewicz, J. Stobie, and A. da Silva, 1995: Documentation of the Goddard Earth Observing System (GEOS) data assimilation system—Version 1. NASA Tech. Memo. 104606, Vol. 4, 44 pp. [Available from Goddard Space Flight Center, Greenbelt, MD 20771.]

Plumb, R. A., 1985: On the three-dimensional propagation of stationary waves. *J. Atmos. Sci.,* **42,** 217–229.

Ropelewski, C. F., and M. S. Halpert, 1987: Global and regional scale precipitation patterns associated with the El Niño/Southern Oscillation. *Mon. Wea. Rev.,* **115,** 1606–1626.

Sadourny, R., 1975: The dynamics of finite difference models of the shallow water equations. *J. Atmos. Sci.,* **32,** 680–689.

Schemm, J.-K., S. Schubert, J. Terry, and S. Bloom, 1992: Estimates of monthly mean soil moisture for 1979–89. NASA Tech. Memo. 104571, 252 pp. [Available from Goddard Space Flight Center, Greenbelt, MD 20771.]

Schubert, S. D., R. B. Rood, and J. Pfaendtner, 1993: An assimilated dataset for earth science applications. *Bull. Amer. Meteor. Soc.,* **74,** 2331–2342.

——, C.-K. Park, C.-Y. Wu, W. Higgins, Y. Kondratyeva, A. Molod, L. Takacs, and R. Rood, 1995: A multi-year assimilation with the GEOS-1 system: Overview and results. NASA Tech. Memo. 104606, Vol. 6, 183 pp. [Available from Goddard Space Flight Center, Greenbelt, MD 20771.]

Suarez, M. J., and L. L. Takacs, 1995: Documentation of the Aries/GEOS Dynamical Core Version 2. NASA Tech. Memo. 104606, Vol. 5, 45 pp. [Available from Goddard Space Flight Center, Greenbelt, MD 20771.]

Takacs, L. L., A. Molod, and T. Wang, 1994: Goddard Earth Observing System (GEOS) general circulation model version 1. NASA Tech. Memo. 104606, Vol. 1, 100 pp. [Available from Goddard Space Flight Center, Greenbelt, MD 20771.]

Ting, M., 1994: Maintenance of northern summer stationary waves in a GCM. *J. Atmos. Sci.,* **51,** 3286–3308.

Valdes, P., and B. J. Hoskins, 1989: Linear stationary wave simulation of the time–mean climatological flow. *J. Atmos. Sci.,* **46,** 2509–2527.

Wallace, J. M., and Q. Jiang, 1987: On the observed structure of the interannual variability of the atmospheric/ocean climate system. *Atmospheric and Oceanic Variability,* H. Cattle, Ed., Royal Meteorological Society, 17–43.

Webster, P. J., 1981: Mechanisms determining the atmospheric response to sea surface temperature anomalies. *J. Atmos. Sci.,* **38,** 554–571.

——, and S. Yang, 1992: Monsoon and ENSO: Selectively interactive systems. *Quart. J. Roy. Meteor. Soc.,* **118,** 877–926.

White, G. H., 1982: An observational study of the Northern Hemisphere extratropical summertime general circulation. *J. Atmos. Sci.,* **39,** 24–40.

World Meteorological Organization, 1995: WMO statement on the status of the global climate in 1994. WMO-No. 826, World Meteorological Organization, Geneva, Switzerland, 20 pp.

Yanai, M., and C. Li, 1994: Mechanism of heating and the boundary layer over the Tibetan Plateau. *Mon. Wea. Rev.,* **122,** 305–323.

——, ——, and Z. Song, 1992: Seasonal heating of the Tibetan Plateau and its effects of the evolution of the Asian summer monsoon. *J. Meteor. Soc. Japan,* **70,** 189–221.

Yasunari, T., 1991: ''The monsoon year''—A new concept of the climatic year in the tropics. *Bull. Amer. Meteor. Soc.,* **72,** 1331–1338.

——, and Y. Seki, 1992: Role of the Asian monsoon on the interannual variability of the global climate system. *J. Meteor. Soc. Japan,* **70,** 177–189.

Ye, D., 1981: Some characteristics of the summer circulation over the Qinghai-Xizang (Tibet) Plateau and its neighborhood. *Bull. Amer. Meteor. Soc.,* **62,** 14–19.